www.czasopisma.pan.pl PAN POLSKA AKADEMIA NAUK www.journals.pan.pl

A R C H I V E S O F M E T A L L U R G Y A N D M A T E R I A L S

Volume 60 2015 Issue 1

DOI: 10.1515/amm-2015-0032

W. WOŁCZYŃSKI*, B. KUCHARSKA**, G. GARZEŁ*, A. SYPIEŃ*, Z. POGODA***, T. OKANE****

PART III. KINETICS OF THE (Zn) – COATING DEPOSITION DURING STABLE AND META-STABLE SOLIDIFICATIONS

CZĘŚĆ III. KINETYKA OSADZANIA POWŁOKI CYNKOWEJ PODCZAS KRYSTALIZACJI STABILNEJ I METASTABILNEJ

Two different steel substrates are applied to the hot dip (Zn) – coating formation. The influence of the substrate composition on the (Zn) – coating thickening is recorded. Morphologies of both coatings are compared to each other. The transition from stable into meta-stable solidification is revealed. The criterion for the competition between stable and meta-stable solidification is applied to justify the analyzed transition.

Keywords: (Zn) – coatings; Fe-Zn phase diagrams; growth kinetics; kinetics law

Zastosowano dwie różne stale jako podłoża dla uzyskania dwu zróżnicowanych powłok (Zn). Dokonano porównania wpływu składu obydwu rodzajów podłoża na kinetykę wzrostu powłok (Zn). Dokonano zestawienia morfologii obydwu powłok. Ujawnione zostało przejście od krystalizacji stabilnej do meta-stabilnej. Zastosowano kryterium współzawodnictwa między krystalizacją stabilną a meta-stabilną dla uzasadnienia analizowanego przejścia.

1. Introduction

Many models for the hot dip coating formation describe the sub-layers formation with the use of the Fe - Zn phase diagram for stable equilibrium, [1-14]. Usually, the kinetics law for the coating growth is formulated, [6], [10], [14]. Some investigations dealing with the reaction at the substrate / coating boundary are also known, [2], [5], [12]. The following phases are formed in the growing coating: Γ_1 – Fe_3Zn; δ – $FeZn_7$, ζ – $FeZn_{13}$ and additionally η – (Zn), [6], [14]. The growth of the δ - $FeZn_7$ – phase can be divided into two separate phenomena: a/ the δ_C – compact phase formation and the δ_P – palisade phase appearance, [7], [14]. The phases Γ_1 – Fe_3Zn; δ – $FeZn_7$, ζ – $FeZn_{13}$ are the products of sub-layers formation during the coating solidification.

The η – Zn – phase is settled, when the substrate is pulling out from the bath, due to the wettability phenomenon, [14]. The current investigation is associated with the Fe-Zn phase diagram which is calculated by means of the professional program ***Pandat Software*** on the basis of the data delivered in Ref. [15].

The recent investigation of the Fe-Zn phase diagram for stable equilibrium, [15], was dedicated, in particular, to the hot-dip galvanizing technology. Therefore, the current model is referred to the above thermodynamic data. One peritectic reaction is visible in the phase diagram for the formation of the δ – phase. Thus, it is obvious that the δ_C – compact phase and the δ_P – palisade phase appear as a product of the same reaction (there are not two independent peritectic reactions for the δ_C, δ_P – phases formation, contrary to the suggestion presented in Ref. [23]).

According to the already known investigations, [16], a few periods of stable or meta-stable solidification appear during the (Zn) – coating formation. In the current model an attempt is made to show that transition from stable into meta-stable solidification occurs at a threshold time exactly at the beginning of the process under investigation. This transition will be justified thermodynamically.

Moreover, the description of the (Zn) – coating stable / meta-stable solidification will be referred to the kinetics law determined for the growth of all phases which form in the coating.

2. Thickening of the hot dip (Zn) – coating

Some experiments of the hot-dip galvanizing were carried out in the industry conditions (CYNKOWNIA ŚLĄSK, Częstochowa-Poland). The experiments were performed with the use of two steel substrates, Fig. 1. The deposition of coatings was completed after 300 [s] of solidification for the first substrate, Fig. 2, and after 120 [s] for the second substrate.

* INSTITUTE OF METALLURGY AND MATERIALS SCIENCE, POLISH ACADEMY OF SCIENCES, 25 REYMONTA STR., 30-059 KRAKÓW, POLAND

** CZĘSTOCHOWA UNIVERSITY OF TECHNOLOGY, FACULTY OF PRODUCTION ENGINEERING AND MATERIALS TECHNOLOGY, 19 ARMII KRAJOWEJ STR., 42-200 CZĘSTOCHOWA, POLAND

*** JAGIELLONIAN UNIVERSITY, FACULTY OF MATHEMATICS AND COMPUTER SCIENCE, 6 ŁOJASIEWICZA STR., 30-348 KRAKÓW, POLAND

**** AIST – NATIONAL INSTITUTE OF ADVANCED INDUSTRIAL SCIENCE & TECHNOLOGY, 305 8568 TSUKUBA, UMEZONO 1-1-1, JAPAN

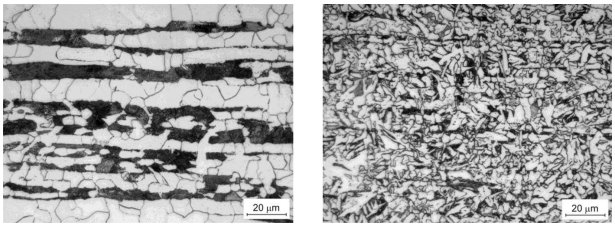

Fig. 1. Morphology of the steel substrates used in the experiments, a/ the S235 – steel (Fe-**0.17C**-1.4Mn-0.55Cu); b/ the S355 – steel (Fe-**0.22C**-1.6Mn-0.55Cu-**0.55Si**); bright areas – *ferrite*, dark areas – *pearlite*

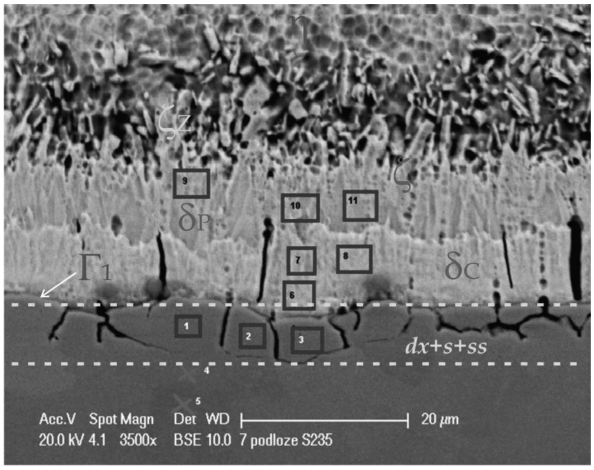

Fig. 2. Morphology of the (Zn) – coating settled on the S235 – steel substrate after 100 [s] of solidification

Some numbered areas, where the Zn – solute redistribution was measured, are marked in Fig. 2. The $(dx + ss + s)$ – zones in which the zinc presence was revealed are also distinguished within the steel substrate (two red crosses are marked to show the zinc absence in this substrate area). Eventually, the location of the different phases in the coating is also shown in Fig. 2.

The results dealing with the evolution of the (Zn) – coating thickness are gathered in Table 1 and Table 2.

TABLE 1
Thickness of the phase sub-layers for the S235 steel substrate; birth time of a given phase corresponds with its sub-layer thickness equal to **0.0** [μm]

time, s	$\Delta\Gamma_1, \mu m$	$\Delta\delta_C, \mu m$	$\Delta\delta_P, \mu m$	$\Delta\zeta, \mu m$	$\Delta\zeta_Z, \mu m$
0	**0.0**				
3		**0.0**	**0.0**		
10	1.2	0.8	1.6		
14				**0.0**	**0.0**
20	1.9	3.0	3.0	2.4	4.0
30	**2.2**	4.0	4.5	3.2	4.6
40	1.9	5.6	5.2	3.9	4.4
60	2.0	7.2	6.8	5.8	4.8
80	2.0	8.4	8.0	6.8	4.5
100	2.0	9.6	9.5	7.8	4.7
120	2.0	9.6	10.0	8.5	4.6
140	2.0	9.6	10.6	9.6	4.5
160	2.0	9.6	11.4	10.3	4.7

TABLE 2
Thickness of the phase sub-layers for the S355 steel substrate; birth time of a given phase corresponds with its sub-layer thickness equal to **0.0** [μm]

time, s	$\Delta\Gamma_1, \mu m$	$\Delta\delta_C, \mu m$	$\Delta\delta_P, \mu m$	$\Delta\zeta, \mu m$	$\Delta\zeta_Z, \mu m$
0	**0.0**				
3		**0.0**	**0.0**		
10	0.4	1.7	3.0	**0.0**	**0.0**
20	**0.7**	2.9	4.8	2.8	2.0
30	0.5	5.3	12.6	4.2	3.2
40	0.55	6.2	14.6	5.4	4.0
60	0.6	7.4	18.8	6.0	5.0
80	0.6	7.4	28.0	5.0	4.8
100	0.6	7.4	35.4	4.8	5.1

The detailed analysis of the thickening / thinning of the Γ_1 – phase sub-layer allows for presenting two adequate curves, Fig. 3.

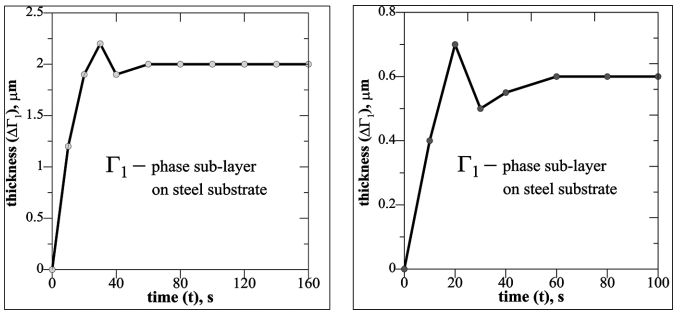

Fig. 3. Tendency of the Γ_1 – phase sub-layer thickening/thinning for; a/ the S235 – steel substrate; b/ the S355 – steel substrate

The stable growth of the Γ – phase occurs for the $0 < t < t_{S/M}$ – time. At the $t_{S/M}$ – time, the stable solidification of the (Zn) – coating transforms into the meta-stable solidification. It is justified because the Γ – phase is no more formed, Fig. 4. Next, some solid / solid transformations only occur (beginning from the $t_{S/M}$ – time). A precipitation of the δ – phase from the Γ – phase appears along with the $t_{S/M} \div t_2$ – period of time. The phenomenon is completed at the t_2 – time, Fig. 4. The reactions: $\Gamma + \delta \rightarrow \Gamma_1$ and $\delta \rightarrow \Gamma_1$ occur within the $t_2 \div t_3$ period of time. The Γ_1 – phase is the stable form beginning from the t_3 – time, Fig. 4.

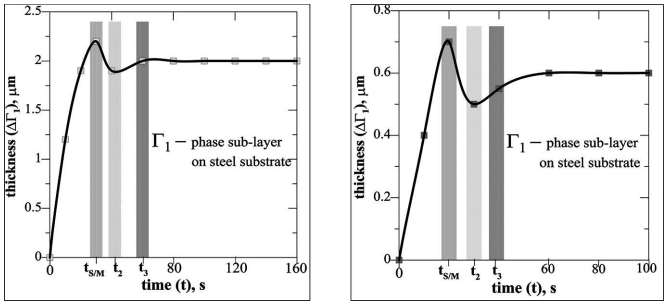

Fig. 4. Selected ranges of the Γ_1 – phase sub-layer thickening/thinning: $0 \div t_{S/M}$; $t_{S/M} \div t_2$; $t_2 \div t_3$; $t > t_3$ for; a/ the S235 – steel substrate; b/ the S355 – steel substrate

It is obvious that the Fe-Zn – phase diagram for stable equilibrium is applicable for the $0 \div t_{S/M}$ – period of time of the (Zn) – coating formation whereas the Fe-Zn – phase diagram for meta-stable equilibrium is valid for the remaining time of the hot dip galvanizing.

3. Calculation of the Fe-Zn phase diagram

The Fe-Zn phase diagram has been calculated by means of the ***Pandat Software***, using the data delivered in Ref. [15], Fig. 5. The sub-layers formed within the $0 \div t_{S/M}$ – period of time have the Zn – solute concentration equal to N_0^S, Fig. 5. It was confirmed by the measurement of the average Zn – solute concentration in the (Zn) – coating; $N_0^S \approx 0.91\,[at.\%\,Zn]$. The phases solidification is accompanied by the peritectic reactions undercooled to the $T_R \approx 450[^\circ C]$, Fig. 5. The concept of the undercooled peritectic reaction has been developed in Ref. [17] and is adapted to the current description.

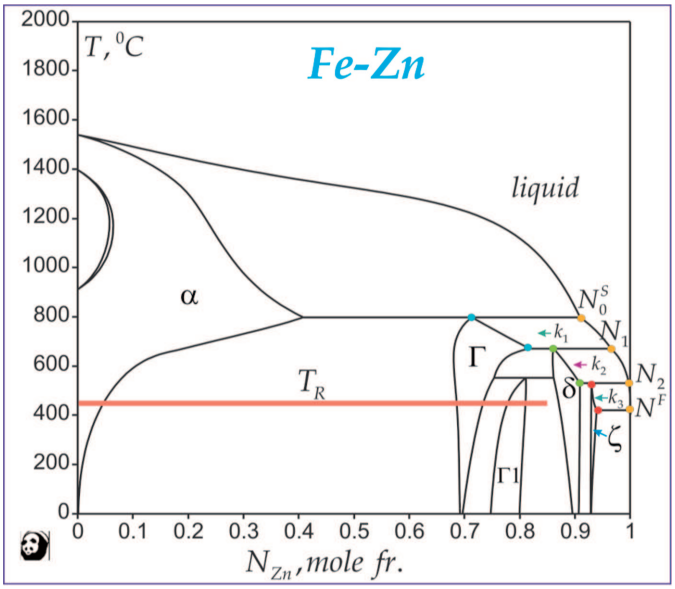

Fig. 5. Fe-Zn phase diagram for stable equilibrium calculated due to the data delivered in Ref. [15], (***Pandat Software***)

The undercooled peritectic reactions which appear within the period of stable solidification are: $liquid\,(N_1) + \Gamma \rightarrow \delta$ and $liquid\,(N_2) + \delta \rightarrow \zeta$, Fig. 5. The primary Γ – phase appears due to the solidification path $N_0^S \div N_1$, Fig. 5, and is not completely consumed during the peritectic reaction. Thus, the Γ – phase sub-layer growth is observed during the stable formation of phases for about 30 seconds in the case of the S235 – steel substrate, Table 1, Fig. 3a. On the other hand, the Γ – phase sub-layer growth is observed during the stable formation of phases for about 20 seconds in the case of the S355 – steel substrate, Table 2, Fig. 3b.

N^F – means the Zn – solute concentration at the end of solidification path and also the Zn – solute concentration in the bath surrounding the steel substrate, Fig. 5. The definition of the N^F – equilibrium solution has already been explained in details on the example of the Ni/Al/Ni joint formation, [18]. The N_0^S or N_0^M – solute concentration for dissolution of the substrate (dissolution always precedes a solidification of some phases in coating or joint, [19], [20], [25]) can also be shown in the phase diagram, Fig. 5 and Fig. 6. The N^F – equilibrium solution is the product of the following reaction: $remaining\ liquid\,(N_2) + liquid\,(Zn) \rightarrow N^F$, which occurs between third and fourteenth second, Table 1, or between third and tenth second, Table 2, (generally, within the time period: $t_B^\delta < t < t_B^\zeta$). It is obvious that the N_0^S is also the nominal solute concentration for the stable solidification. Analogously, the N_0^M is the nominal solute concentration for the meta-stable solidification.

The solute concentration in the dissolution zone must be equal to the nominal solute concentration for solidification as it results from the mass balance. It is explained in Fig. 7.

The $t_B^\delta = 3$ – parameter is the time of the δ – phase birth (nucleation), and the $t_B^\zeta = 14$ – parameter is the time of the ζ – phase birth, Table 1. The $t_B^\delta = 3$ – parameter is the time of the δ – phase birth (nucleation), and the $t_B^\zeta = 10$ – parameter is the time of the ζ – phase birth, Table 2.

The stable period of solidification is transformed into meta-stable solidification at the $t_{S/M}$ – time, Fig. 4. At this threshold time the Γ – phase appearance is no more observed, Table 1, Table 2 and solidification should be referred to the phase diagram for meta-stable equilibrium. The phase diagram for meta-stable equilibrium, calculated by means of the ***Pandat Software***, is presented in Fig. 6.

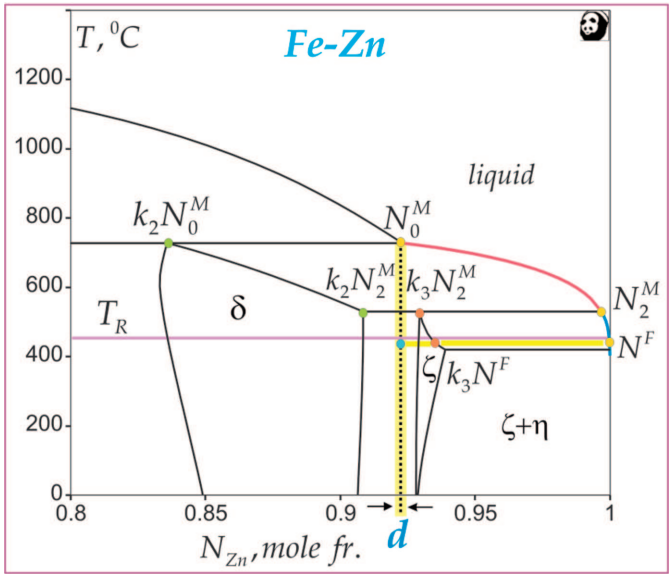

Fig. 6. Fe-Zn phase diagram for meta-stable equilibrium calculated due to the data delivered in Ref. [15], (***Pandat Software***); the red *liquidus* lines corresponds with the δ – phase sub-layer formation due to the partitioning which is completed by the undercooled peritectic reaction: $\delta\left(k_2N_2^M\right) + liquid\left(N_2^M\right) \rightarrow \zeta\left(k_3N_2^M\right)$; the blue *liquidus* lines corresponds with the ζ – phase sub-layer formation by the partitioning; $N^F \div N_0^M$ is the dissolution path (yellow line); $d\left(N_0^M\right)$ is the localization of the dissolution zone in the phase diagram

The $N_0^S \rightarrow N_0^M$ – transition occurs at the – $t_{S/M}$ time, with $N_0^M \approx 0.925\,[at.\%]$, Fig. 6, whereas, $N_0^S \approx 0.91\,[at.\%]$, Fig. 5. Both concentrations are determined by the mass balance measurements.

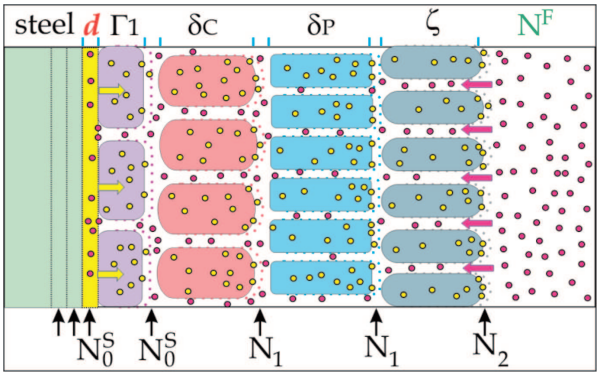

Fig. 7. Model for the (Zn) – coating formation during the hot dip galvanizing; d – dissolution zone formed at the surface of the steel substrate; N^F – equilibrium solution of the Fe in the zinc bath; N_0^S – solute concentration in the dissolution zone ensures the stable solidification of all sub-layers in the (Zn) – coating due to the bulk diffusion (yellow arrows); the N^F – solution diffuses towards the steel to form the dissolution zone due to the boundary diffusion (red arrows); both flows are equal to each other in the current model; contrary to Ref. [23] the same peritectic reaction leads to formation of both varieties of the δ – phase sub-layers ($\delta_C + \delta_P$); left to the d – zone the supersaturated zone (ss) and saturated zone (s) are marked by the arrows

The meta-stable solidification is the winner in the competition at time, $t_{S/M}$, Fig. 4. This victory can be justified theoretically through the satisfaction of the inequality $T_\delta^* > T_\Gamma^*$, Fig. 8. According to this criterion, the δ – phase formation is the winner in the competition because the δ – phase has a higher temperature of its s/l interface, in comparison with the s/l interface temperature of the Γ – phase formation, [22], [24]. The intersections of the N_0^S – solute concentration (vertical dotted line) with the *solidus* lines of Γ – phase and δ – phase, respectively, yield the inequality presented in Fig. 8.

In the consequence, the δ – phase solidification substitutes the Γ – phase solidification as visible in Fig. 7.

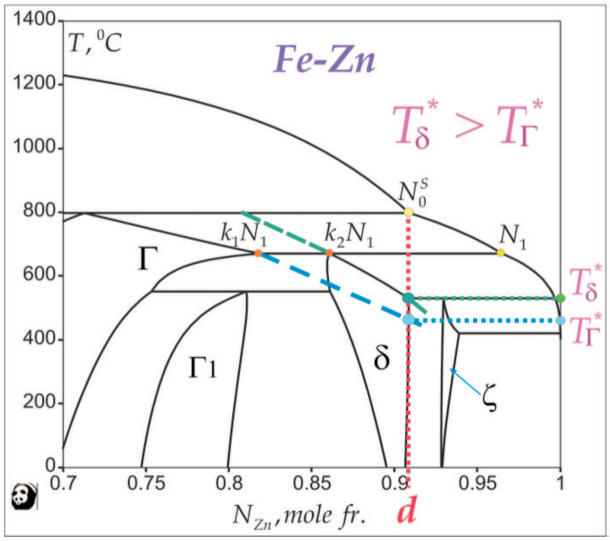

Fig. 8. Application of the criterion of the higher temperature of the s/l interface to the description of the hot dip galvanizing technology; T_Γ^* – temperature of the s/l interface for the Γ – phase; T_δ^* – temperature of the s/l interface for the δ – phase solidification

4. Kinetics of the (Zn) – coating growth

The measurements of the sub-layers thickness, Table 1, Table 2 allow for making comparison between the phases growth with respect to time, Fig. 9-17.

The thickening of the δ_C – phase sub-layer is interrupted at a time characteristic (typical) for a given substrate used in experiment, Table 1, Table 2. This interruption is shown in Fig. 9.

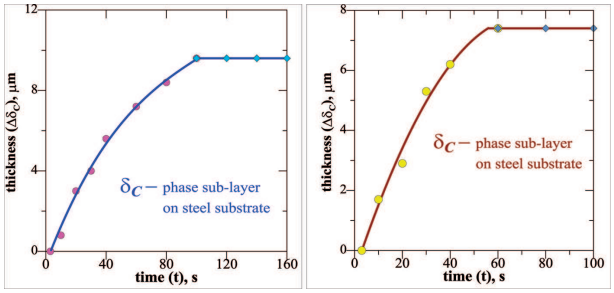

Fig. 9. Tendencies (a/ red and blue points; b/ yellow and blue points) of the δ_C – phase sub-layer thickening within the (Zn) – coating settled on a/ the S235 steel, b/ the S355 steel substrate

Contrary to the δ_C – phase sub-layer thickening, the thickening of the δ_P – phase sub-layer does not interrupt, Table 1, Table 2. However, the interrupted growth of the δ_C – phase sub-layer influences the δ_P – phase sub-layer formation. Thereby, the tendencies of the δ_P – phase sub-layer thickening is divided into two ranges, Fig. 10. Both ranges are well visible, particularly in Fig. 10a.

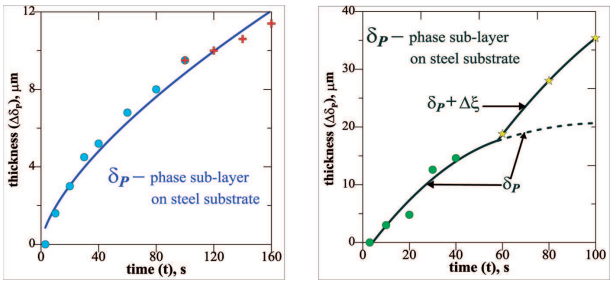

Fig. 10. Tendencies of the δ_P – phase sub-layer thickening within the (Zn) – coating settled on: a/ the S235 steel substrate (blue and red points), b/ the S355 steel substrate (green and yellow points)

An analysis of both δ_C and δ_P sub-layers growth allows for determining the t_0 – time at which the δ_C – phase sub-layer growth is completed, Fig. 11.

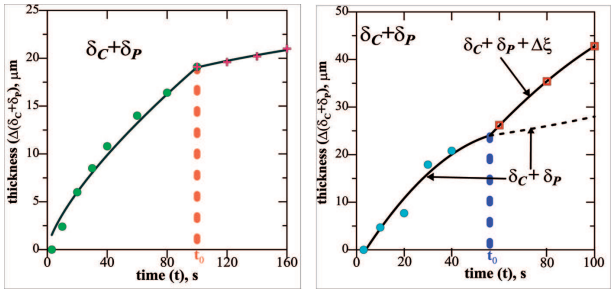

Fig. 11. Kinetics of the $(\delta_C + \delta_P)$ – phases double-layer growth in the (Zn) – coating settled on: a/ the S235 steel substrate, b/ the S355 steel substrate

The t_0 – time is equal to about 100 seconds for the S235 steel substrate, Fig. 11a and equal to about 56 seconds for the S355 steel substrate, Fig. 11b.

It is obvious that the δ – phase follows two modes of growth. When δ – phase appears as the δ_C – phase variant, it has another morphology than that revealed for the δ_P – phase variant.

The morphology of the δ_C – phase differs from that of the δ_P – phase because the s/l interface of the δ_C – phase sub-layer is modified by the products of the flux disintegration into gaseous form (chlorine bubbles) and possible transformation into ash/slag. On the other hand, the δ_P – phase sub-layer is formed in the local contact with the pure (Zn) – bath which does not contain the gaseous bubbles and ash/slag particles.

Both analyzed phases, δ_C and δ_P, are the product of the same undercooled peritectic reaction as visible in the phase diagram, Fig. 5, when $t \leqslant t_{S/M}$. The mentioned phases are the product of the Zn - solute partitioning as visible in the phase diagram, Fig. 6, when $t > t_{S/M}$.

The ζ – phase sub-layer thickening is shown in Fig. 12.

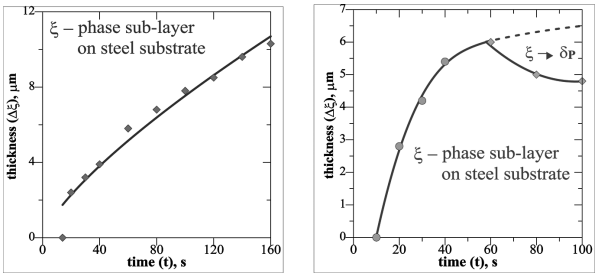

Fig. 12. Tendency of the ζ – phase sub-layer thickening in the (Zn) – coating settled on: a/ the S235 – steel substrate, b/ the S355 – steel substrate

It is well visible that the S355 steel substrate promotes the appearance of the $\zeta \rightarrow \delta_P$ transformation at the fifteenth six – sixteenth seconds of the ζ – phase sub-layer growth. This is the so-called "*mantis*" phenomenon revealed for the Ni/Al/Ni interconnections formation, [18]. On the other hand, this solid / solid transformation did not appear during the (Zn) – coating formation on the S235 steel substrate within the period of time, $0 \div 160$ seconds.

The kinetics of the $\zeta_Z = \zeta + \eta$ – phases sub-layer is presented in Fig. 13, Fig. 14.

The ζ_Z – sub-layer is intensively formed till the $t_{S/M}$ – time for the S235 – steel substrate, Fig. 13. Beginning from the $t_{S/M}$ – time the ζ_Z – sub-layer growth oscillates between thickening and thinning. The ζ_Z - sub-layer is intensively formed till the t_0 – time for the S355 – steel substrate, Fig. 14. Beginning from the t_0 – time the ζ_Z – sub-layer growth also oscillates between thickening and thinning. It can be concluded that the observed thinning of the ζ_Z – phase sub-layer leads to the detachment of some sub-layer fragments. Some of the ζ – phase cells detached off (separated) from the ζ_Z – sub-layer flow all the time into the zinc bath. They become so heavy that settle down on the bottom to form a zinc silt. However, other ζ – phase cells appear within the ζ_Z – sub-layer for time, $t > t_{S/M}$, Fig. 13 and for the time $t > t_0$, Fig. 14.

It seems that the optimal thickness of the ζ_Z – sub-layer is conserved in the coating for a given condition of the hot dip galvanizing. Moreover, this optimal thickness depends on the chemical composition and morphology of the substrate used in the technology.

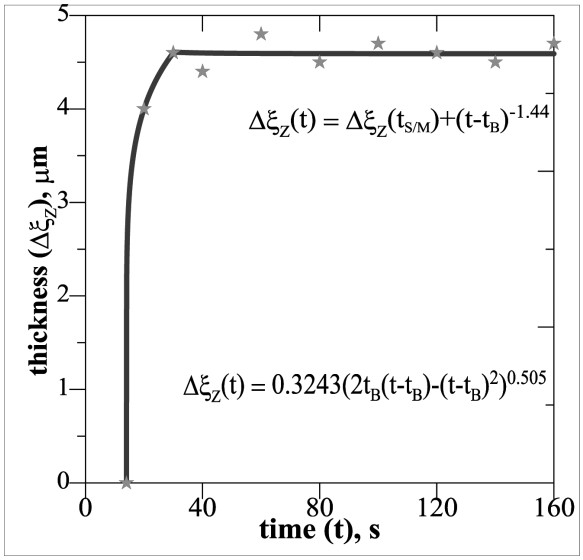

Fig. 13. Kinetics of the ζ_Z – sub-layer growth in the (Zn) – coating settled on the S235 – steel substrate

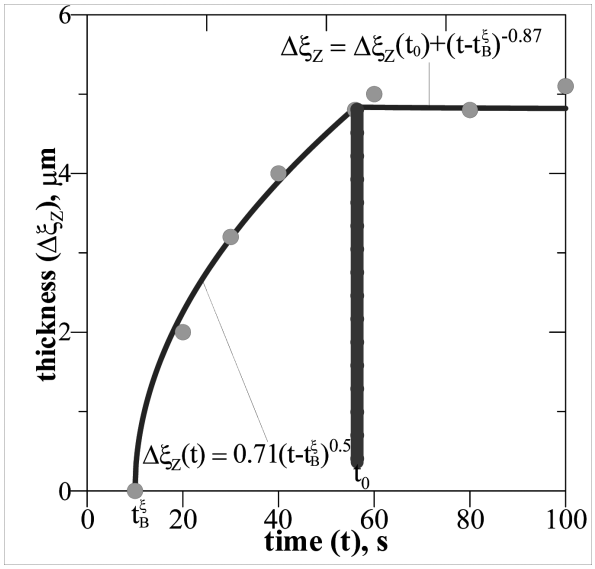

Fig. 14. Kinetics of the ζ_Z – sub-layer growth in the (Zn) – coating settled on the S355 – steel substrate

The common thickening of the sub-layers not perturbed by the detachment, and which results strictly from solidification, is shown in Fig. 15, Fig. 16 and Fig. 17.

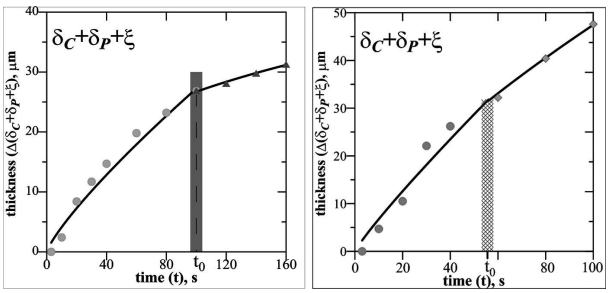

Fig. 15. Tendency of the δ_C, δ_P and ζ – phase sub-layers thickening in the (Zn) – coating settled on: a/ the S235 – steel substrate, b/ the S355 – steel substrate

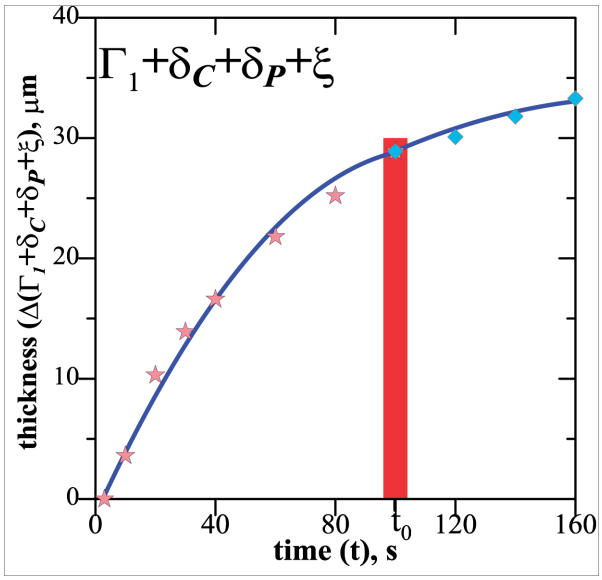

Fig. 16. Kinetics of the Γ_1, δ_C, δ_P and ζ – phase sub-layers growth in the (Zn) – coating settled on the S235 – steel substrate

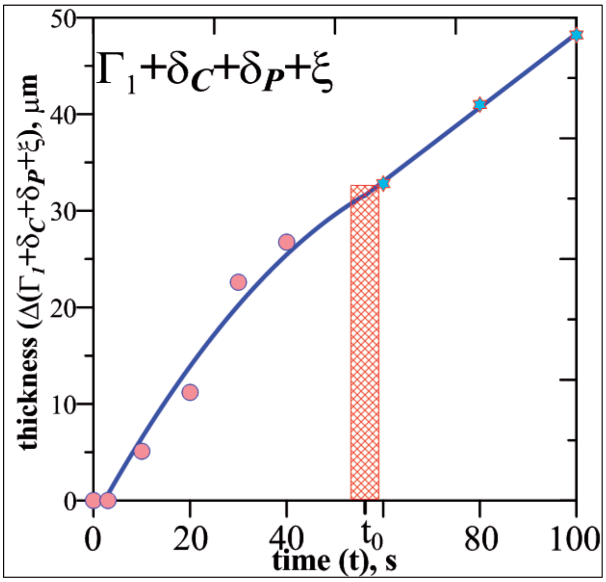

Fig. 17. Kinetics of the Γ_1, δ_C, δ_P and ζ – phase sub-layers growth in the (Zn) – coating settled on the S355 – steel substrate

5. Concluding remarks

In the case of the stable solidification both δ – phases ($\delta_C + \delta_P$) are formed in a complicated way. Really, the δ – phases are formed due to the peritectic reaction udercooled to the T_R – temperature. The peritectic reaction requires the diffusion to be occurred. It delays the solidification. Therefore, the stable solidification transforms into the meta-stable solidification as stated in Fig. 4. In the case of the meta-stable solidification the formation of the Γ_1 – phase disappears and the δ – phases formation occurs in a simplest way, due to the *liquidus* →*solidus* partitioning of zinc, only, Fig. 6 (red *liquidus* line).

The partitioning promotes the creation of the zinc concentration gradient in the cells. Thus, the diffusion into the solid forms at the same time, as explained by the model for the solute redistribution, [21]. Zinc redistribution appears and can be measured by the EDS technique as shown in Fig. 18.

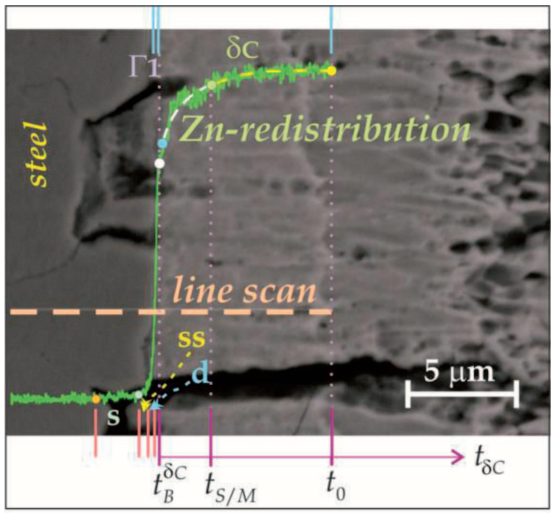

Fig. 18. Zn – solute redistribution in the vicinity of the substrate / coating interface; the postulated localizations of: *d* – dissolution zone, *ss* – supersaturation zone and *s* – saturation zone in the S235 – steel substrate; $t_B^{\delta C}$ – time of the δ_C – phase birth (nucleation)

The revealed Zn – solute presence in the substrate within the distinguished *ss* - supersaturation and *s* - saturation zones, Fig. 18, corresponds well with the adequate predictions of these zones localization, Fig. 7.

Generally, the results gathered in Table 1 and Table 2 reveal the influence of two different substrates (influence of their structure and elements content) on the sub-layers growth kinetics, Fig. 11, Fig. 13, Fig. 14 and Fig. 16.

The kinetics law for the coating growth has the following general form which is given by a power function:

$$\Delta p = k_p\, t^m \quad 0.5 \leqslant m \leqslant 1 \tag{1}$$

It is assumed in the current model that the index of the power satisfies the following inequality: $0.5 \leqslant m \leqslant 1$ in the kinetics law Eq. (1), where $p = \Gamma, \delta, \zeta$. The index of the power is $m = 1$, when the diffusion occurs along the external channels, and $m = 0.5$, when the bulk diffusion across the cells, is effective, only, [26]. Thereby,

A/ in the case of the S235 – steel substrate (Fe-**0.17C** -1.4Mn-0.55Cu) the above law, Eq. (1), can be presented as follows:

a/ for the Γ_1 – phase sub-layer formation, Fig. 3a, an elliptical relationship can be used, (it contains the power function, Eq. (1) by itself):

$$\Delta\Gamma_1(t) = \lambda^{\Gamma}(t) = G_{235}\frac{\lambda^{\Gamma}(t_{S/M})}{t_K}\left[2\,t_K\,t - t^2\right]^g, \quad t \in \left[t_B^{\Gamma 1}, t_K\right] \tag{2a}$$

where $G_{235} = 1.05$, and $g = 0.5$ on the basis of the experimental results gathered in Table 1, with $t_B^{\Gamma 1} = 0$ [s].

b/ for the δ_C – phase sub-layer formation, Fig. 9a, the power function is:

$$\Delta\delta_C(t) = \lambda^{\delta C}(t) = C_{235}\left(t - t_B^{\delta}\right)^c, \quad t \in \left[t_B^{\delta}, t_0\right] \tag{3a}$$

where $C_{235} = 0.6$, and $c = 0.606$ on the basis of the experimental results gathered in Table 1.

c/ for the δ_P – phase sub-layer formation, Fig. 10a, the power function is:

$$\Delta\delta_P(t) = \lambda^{\delta P}(t) = P_{235}\left(t - t_B^{\delta}\right)^p, \quad t \in \left[t_B^{\delta}, t_K\right] \tag{4a}$$

where $P_{235} = 0.80$, and $p = 0.53$ on the basis of the experimental results gathered in Table 1.

d/ for the $\delta = \delta_C + \delta_P$ – phase sub-layers formation, Fig. 11a, the power function can be used to describe the general tendency of the δ – phase sub-layer thickening:

$$\Delta\left[\delta_C + \delta_P\right](t) = \lambda^{\delta}(t) = L_{235}\left(t - t_B^{\delta}\right)^l, \quad t \in \left[t_B^{\delta}, t_0\right] \tag{5a}$$

where $L_{235} = 1.35$, and $l = 0.58$ on the basis of the experimental results gathered in Table 1.

$$\Delta\left[\delta_C + \delta_P\right](t) = \lambda^{\delta}(t) = \Delta\left[\delta_C + \delta_P\right](t_0) + R_{235}(t - t_0)^r, \quad t \in [t_0, t_K] \tag{6a}$$

where $R_{235} = 0.15$, and $r = 0.65$ on the basis of the experimental results gathered in Table 1, with, $t_0 = 100$ [s], $t_K = 300$ [s], and $t_B^{\delta} = 3$ [s].

e/ for the ζ – phase sub-layer formation, Fig. 12a, the power function is:

$$\Delta\zeta(t) = \lambda^{\zeta}(t) = Z_{235}\left(t - t_B^{\zeta}\right)^z, \quad t \in \left[t_B^{\zeta}, t_K\right] \tag{7a}$$

where $Z_{235} = 0.67$, and $z = 0.55$ on the basis of the experimental results gathered in Table 1, with $t_B^{\zeta} = 14$ [s].

f/ for the ζ_Z – sub-layer formation, Fig. 13, the adequate function is as follows:

$$\Delta_{\zeta Z}(t) = \lambda^{\zeta Z}(t) = J_{235}\left[2\,t_B^{\zeta}\left(t - t_B^{\zeta}\right) - \left(t - t_B^{\zeta}\right)^2\right]^j, \quad t \in \left[t_B^{\zeta}, t_{S/M}\right] \tag{8a}$$

$$\Delta_{\zeta Z}(t) = \lambda^{\zeta Z}(t) = \left(t - t_B^{\zeta}\right)^{-1.44} + \Delta_{\zeta Z}(t_{S/M}), \quad t \in [t_{S/M}, t_K] \tag{9a}$$

where $J_{235} = 0.3243$, and $j = 0.505$ on the basis of the experimental results gathered in Table 1.

g/ for the $[\Gamma_1 + \delta_C + \delta_P + \zeta]$ – sub-layers formation, Fig. 16, the power function is:

$$\Delta\left[\Gamma_1 + \delta_C + \delta_P + \zeta\right](t) = \lambda^{\Gamma_1 + \delta_C + \delta_P + \zeta}(t) = Y_{235}(t)^y \quad t \in [0, t_0] \tag{10a}$$

where $Y_{235} = 2$, and $y = 0.58$ on the basis of the experimental results gathered in Table 1.

$$\Delta\left[\Gamma_1 + \delta_C + \delta_P + \zeta\right](t) = \lambda^{\Gamma_1 + \delta_C + \delta_P + \zeta}(t) = \Delta\left[\Gamma_1 + \delta_C + \delta_P + \zeta\right](t_0) + U_{235}(t - t_0)^u, \quad t \in [t_0, t_K]$$

where $U_{235} = 0.3$, and $u = 0.6$ on the basis of the experimental results gathered in Table 1.

The predicted presence of the flux at the δ_C – interface, [25] and [26], can make the growth of the δ_C – phase more difficult. Indeed, the bulk diffusion across the δ_C – cells is not sufficiently intensive. Therefore, the m – power index in the kinetics law is not equal to 0.5. In fact, $m = 0.606$ for the δ_C – phase growth, Eq. (3a). It is obvious that the channels (boundary diffusion) has also to be exploited to some extent in the δ_C – phase growth. On the other hand, $m = 0.530$ in the δ_P – phase kinetics law, Eq. (4a). Thus, the bulk diffusion across the δ_P – cells is dominant in the δ_P – phase sub-layer growth, since the power index $m \to 0.5$.

Therefore, the power index is $m = 0.580$ for the $[\delta_C + \delta_P]$ – phases growth, Eq. (5a), $(m_{\delta P} < m_{(\delta C + \delta P)} < m_{\delta C})$.

B/ in the case of the S355 – steel substrate (Fe-**0.22C**-1.6Mn-0.55Cu-**0.55Si**) the mentioned law, Eq. (1), can be presented as follows:

a/ for the Γ_1 – phase sub-layer formation, Fig. 3b, an elliptical relationship can be used (but it contains a power function, Eq. (1) in itself):

$$\Delta\Gamma_1(t) = \lambda^{\Gamma}(t) = G_{355}\frac{\lambda^{\Gamma}(t_{S/M})}{t_K}\left[2\,t_K\,t - t^2\right]^g, \quad t \in \left[t_B^{\Gamma 1}, t_K\right] \tag{2b}$$

where $G_{355} = 1.07$, and $g = 0.5$ on the basis of the experimental results gathered in Table 2, with $t_B^{\Gamma 1} = 0$ [s].

b/ for the δ_C – phase sub-layer formation, Fig. 9b, a power function, Eq. (1) is:

$$\Delta\delta_C(t) = \lambda^{\delta C}(t) = C_{355}\left(t - t_B^{\delta}\right)^c, \quad t \in \left[t_B^{\delta}, t_0\right] \tag{3b}$$

where $C_{355} = 0.52$, and $c = 0.67$ on the basis of the experimental results gathered in Table 2 with $t_B^{\delta} = 3$ [s].

c/ for the δ_P – phase sub-layer formation, Fig. 10b, a power function, Eq. (1) is:

$$\Delta\delta_P(t) = \lambda^{\delta P}(t) = P_{355}\left(t - t_B^{\delta}\right)^p, \quad t \in \left[t_B^{\delta}, t_K\right] \tag{4b}$$

where $P_{355} = 0.65$, and, $p = 0.84$ on the basis of the experimental results gathered in Table 2.

d/ for the $\delta = \delta_C + \delta_P$ – phase sub-layers formation, Fig. 11b, a power function, Eq.(1), can be used to describe the general tendency of the δ – phase sub-layer thickening:

$$\Delta\left[\delta_C + \delta_P\right](t) = \lambda^{\delta}(t) = L_{355}\left(t - t_B^{\delta}\right)^l, \quad t \in \left[t_B^{\delta}, t_0\right] \tag{5b}$$

where $L_{355} = 1.546$, and $l = 0.7$ on the basis of the experimental results gathered in Table 2.

$$\Delta\left[\delta_C + \delta_P + \Delta\zeta\right](t) = \lambda^{\delta}(t) = \Delta\left[\delta_C + \delta_P + \Delta\zeta\right](t_0) + R_{355}\left(t - t_{\zeta\to\delta}\right)^r, \quad t \in [t_0, t_K] \tag{6b}$$

where $R_{355} = 0.697$, and $r = 0.86$ on the basis of the experimental results gathered in Table 2 with $t_{\zeta\to\delta} \approx t_0$, $t_0 = 56$ [s], $t_K = 120$ [s], and $t_B^{\delta} = 3$ [s].

e/ for the ζ – phase sub-layer formation, Fig. 12b, a power function, Eq. (1), is:

$$\Delta\zeta(t) = \lambda^{\zeta}(t) = Z_{355}\left(t - t_B^{\zeta}\right)^z, \quad t \in \left[t_B^{\zeta}, t_K\right] \tag{7b}$$

where $Z_{355} = 0.847$, and $z = 0.5$ on the basis of the experimental results gathered in Table 2, with $t_B^{\zeta} = 10$ [s].

f/ for the ζ_Z – sub-layer formation, Fig. 14, the function is as follows:

$$\Delta_{\zeta Z}(t) = \lambda^{\zeta Z}(t) = J_{355}\left(t - t_B^{\zeta}\right)^j, \quad t \in \left[t_B^{\zeta}, t_{\zeta\to\delta}\right] \tag{8b}$$

where $J_{355} = 0.71$, $j = 0.5$ on the basis of the experimental results gathered in Table 2.

$$\Delta_{\zeta Z}(t) = \lambda^{\zeta Z}(t) = \Delta_{\zeta Z}\left(t_{\zeta\to\delta}\right) + \left(t - t_B^{\zeta}\right)^{-0.87}, \quad t_{\zeta\to\delta} < t \leqslant t_K \tag{9b}$$

g/ for the $[\Gamma_1 + \delta_C + \delta_P + \zeta]$ – sub-layers formation, Fig. 17, a power function, Eq. (1) is:

$$\Delta[\Gamma_1 + \delta_C + \delta_P + \zeta](t) = \lambda^{\Gamma_1+\delta_C+\delta_P+\zeta}(t) = Y_{355}(t)^y \quad t \in [0, t_0] \tag{10b}$$

where $Y_{355} = 2.275$, and $y = 0.66$ on the basis of the experimental results gathered in Table 2.

$$\Delta[\Gamma_1 + \delta_C + \delta_P + \zeta](t) = \lambda^{\Gamma_1+\delta_C+\delta_P+\zeta}(t) = \Delta[\Gamma_1 + \delta_C + \delta_P + \zeta](t_0) + U_{355}(t - t_0)^u, \quad t_0 < t \leqslant t_K$$

where $U_{355} = 1.935$, and u =0.7 on the basis of the experimental results gathered in Table 2.

The analyzed settlement of the (Zn) – coating on the steel substrate differs from each other.

A/ In the case of the S235 steel substrate with a moderate content of carbon and no silicon, all the indexes of the power satisfy the inequality: $0.5 \leqslant m \leqslant 1$. In particular, for

a/ the Γ_1, δ_P, ζ – phases,

the index of the power is close to 0.5. It suggests the occurrence of the bulk diffusion of the zinc towards the s/l interface of the respective sub-layers, Eq. (2a), Eq. (4a), Eq. (7a) and Eq. (8a),

b/ the δ_C – phase,

the index of the power is a little bit greater than the ideal value equal to 0.5. It means that the both diffusions (bulk diffusion and boundary diffusion along channels) occurred during formation of this sub-layer, Eq. (3a). It was caused by the presence of the flux located at the s/l interface. This flux changes the mechanical equilibrium at the s/l interface and therefore the morphology of the δ_C – phase differs from that of the δ_P – phase though both phases are of the same origin (of the same partitioning), Fig. 6.

B/ In the case of the S355 steel substrate with elevated content of carbon and significant presence of silicon, all the indexes of the power satisfy the inequality: $0.5 \leqslant m \leqslant 1$. In particular, for

a/ the Γ_1, ζ – phases,

the index of the power is close to 0.5. It suggests the occurrence of the bulk diffusion of the zinc towards the s/l interface of the respective sub-layers, Eq. (2b), Eq. (7b) and Eq. (8b),

b/ the δ_C – phase,

the index of the power is a little bit greater than the ideal value equal to 0.5. It means that the both diffusions (bulk diffusion and boundary diffusion along channels) occurred during formation of this sub-layer, Eq. (3b). It was caused by the presence of the flux located at the s/l interface.

c/ the δ_P – phase,

the index of the power is rather close to unity, Eq. (4b), $m \to 1$. It means that the s/l interface of the δ_P – phase sub-layer was blocked by the carbon and silicon which diffuses towards the zinc bath, but were settled on the δ_P – phase sub-layer interface. Therefore, the intensive diffusion of the zinc through the channels is expected for the δ_P – phase formation.

It can be concluded that the (Zn) – coating formation on the S355 – steel substrate is difficult, however possible for 2 minutes' duration of the hot dip galvanizing. After this period of time, the carbon and silicon diffusion into the coating promotes the delamination of the coating from the steel substrate. It can be concluded that the carbon and silicon content in the coating reached the critical values which block the effective sub-layers formation. The 2 minutes' settlement of the (Zn) – coating on the S355 steel substrate is confirmed by the result of experiment made in the industry condition, Table 2.

Even, the behavior of the ζ_Z – phase formation differs from each other. Therefore, the kinetics law for the ζ_Z – phase is described by different types of function. In the case of the S235 – steel substrate the elliptical function is applicable, Eq. (8a), Fig. 13. Contrary, in the case of the S355 – steel substrate the analogous description is obtained by means of the power function, Eq. (8b), Fig. 14.

The presence of the flux as well as silicon and elevated content of carbon in the S355 – steel makes the δ_C – phase growth more difficult than the growth of the same phase on the S235 – steel substrate. Therefore, $m_{\delta C}^{235} < m_{\delta C}^{355}$, Eq. (3a) and Eq. (3b). It results in the greater contribution of the boundary diffusion in the case of the (Zn) – coating settlement on the S355 – steel substrate. Therefore, the diffusion for dissolution is perturbed by the diffusion for solidification because both occur along the same channels but in the inverse directions. Thus, it involves a substantial deviation from the ideal model of coating formation, Fig. 7.

In the both cases, the power index satisfies the inequality: $m_{\delta P} < m_{(\delta C+\delta P)} < m_{\delta C}$, for the $[\delta_C + \delta_P]$ – phases growth.

The δ – phases formation is split into two sub-phases growth due to the use of flux in the hot dip galvanizing technology, Table 1, Table 2. Therefore, the δ_P – phase appears in the coating, only, when the flux evaporation is completed at the t_0 – time, Fig. 9.

The growth of the ζ – phase sub-layer is not essentially perturbed by the presence of flux in the bath, Eq. (7a), Eq. (7b). It can be assumed that the thickening of the ζ – phase sub-layer is the result of the bulk diffusion, only, ($m \approx 0.5$), according to the model for the ideal formation of a coating, Fig. 7.

Generally, the kinetics of the ideal dissolution, Fig. 7, is continuously retarded by the cluttering of the external channels (channels between cells within a given sub-layer) and by the diffusion distances which increase during coating settlement. In the current model, the ideal substrate dissolution occurs with the use of the external channels (boundary diffusion), only. The ideal thickening (solidification) is possible due to the bulk diffusion (across the cells), Fig. 7. In reality, rather a combination of both types of diffusion are exploited for the substrate dissolution or for the sub-layers thickening.

The S355 – substrate steel contains 0.22 [%C] and 0.55 [%Si], whereas the S235 substrate steel does not contain silicon. Moreover, the morphologies of both substrates differ from each other, Fig. 1a, Fig. 1b.

The differences in elements content as well as in morphologies cause the following consequences:

A/ for the (Zn) – coating settled on the S235 – steel substrate with $t_K = 300$ [s],

$t_{S/M} \approx 30$[s]; $t_B^{\delta} \approx 3$ [s]; $t_B^{\zeta} \approx 14$ [s]; $t_0 \approx 100$ [s]; $t_{\zeta\to\delta} \gg t_0$; $t_{\zeta\to\delta} > t_K$

B/ for the (Zn) – coating deposited on the S355 – steel substrate with $t_K = 120$ [s],

$t_{S/M} \approx 20$[s]; $t_B^{\delta} \approx 3$ [s]; $t_B^{\zeta} \approx 10$ [s]; $t_0 \approx 56$ [s]; $t_{\zeta\to\delta} \approx t_0$; $t_{\zeta\to\delta} < t_K$

where t_K is the time usually applied to the hot dip galvanizing of the analyzed steel substrates by the plant CYNKOWNIA ŚLĄSK, Częstochowa-Poland.

REFERENCES

[1] A. Bohran-Tavakoli, Formation and growth of the δ 1 phase in the Fe-Zn system. Part 1. Zeitschrift für Metallkunde **75**, 350-355 (1984).

[2] J. Inagaki, M. Sakurai, T. Watanabe, Alloying reactions in hot dip galvanizing and galvannealing processes. ISIJ International **35**, 1388-1393 (1995).

[3] C.E. Jordan, A.R. Marder, Fe-Zn phases formation in interstitial – free steels hot-dip galvanized at 450°C. Journal of Materials Science **32**, 5593-5602 (1997).

[4] J.D. Culcasi, P.R. Sere, C.I. Elsner, A.R. Sarli, Control of the growth of zinc – iron phases in the hot dip galvanizing process. Surface and Coatings Technology **122**, 682-686 (1999).

[5] E. Scheil, H. Wurst, Über die reaktionen des eisens mit flüssigem zink. Zeitschrift für Metallkunde **29**, 225-228 (1937) (in German).

[6] D. Kopyciński, Krystalizacja faz międzymetalicznych i cynku na żelazie oraz na jego nisko- i wysokowęglowych stopach podczas procesu cynkowania, Rozprawy Monografie AGH, **149**, 131 (2006) (in Polish).

[7] M.A. Ghoniem, K. Lohberg, Über die feuerverzinkung entstenden δ 1p und δ 1k schichten, Metall **26**,1026-1030 (1972) (in German).

[8] P.J. Gelliings, E.W. Bree, G. Gierman, Synthesis and characterization of homogeneous intermetallic Fe-Zn compounds. Part1. Zeitschrift für Metallkunde **70**, 312-314 (1979).

[9] P.J. Gelliings, E.W. Bree, G. Gierman, Synthesis and characterization of homogeneous intermetallic Fe-Zn compounds. Part 2. Zeitschrift für Metallkunde **70**, 315-317 (1979).

[10] C.E. Jordan, A.R. Marder, Morphology development in hot-dip galvanneal coatings. Metallurgical and Materials Transactions **25A**, 937-947 (1994).

[11] C.R. Xavier, U.R. Seixas, P.R. Rios, Further experimental evidence to support a simple model for iron enrichment in hot-dip galvanneal coatings on IF steel sheets. ISIJ International **36**, 1316-1317 (1996).

[12] M. Danielewski, Diffusion in multicomponent systems, Archives of Metallurgy and Materials **49**, 189-200 (2004).

[13] M. Zapponi, A. Quiroga, T. Perez, Segregation of alloying elements during the hot-dip coating solidification process, Surface and Coatings Technology **122**, 18-20 (1999).

[14] J. Maćkowiak, N.R. Short, Metallurgy of galvanized coatings, International Metals Reviews **237**, 1-19 (1979).

[15] W. Xiong, Y. Kong, Y. Dub, L. Zikui, M. Selleby, S. Weihua, Thermodynamic investigation of the galvanizing systems, I: Refinement of the thermodynamic description for the Fe-Zn system, CALPHAD: Computer Coupling of Phase Diagrams and Thermo-Chemistry **33**, 433-440 (2009).

[16] P. Perrot, J.C. Tissier, J.Y. Dauphin, Stable and metastable equilibria in the Fe-Zn-Al system at 450°C, Zeitschrift für Metallkunde **83**, 786-790 (1992).

[17] Y.K. Chuang, D. Reinisch, K. Schwerdtfeger, Kinetics of diffusion controlled peritectic reaction during solidification of iron-carbon alloys, Metallurgical Transactions **6A**, 235-238 (1975).

[18] W. Wołczyński, T. Okane, C. Senderowski, D. Zasada, B. Kania, J. Janczak-Rusch, Thermodynamic justification for the Ni/Al/Ni joint formation by a diffusion brazing, International Journal of Thermodynamics **14**, 97-105 (2011).

[19] I. Tuah-Poku, M. Dollar, T. Massalski, A study of transient phase bonding process applied to a Ag/Cu/Ag sandwich joint, Metallurgical Transactions **19A**, 675-686 (1988).

[20] W. Wołczyński, J. Janczak-Rusch, J. Kloch, T. Rutti, T. Okane, A model for solidification of intermetallic phases from Ni-Al system and its application to diffusion soldering, Archives of Metallurgy and Materials **50**, 1055-1068 (2005).

[21] W. Wołczyński, Back-diffusion phenomenon during the crystal growth by the Bridgman method, Chapter 2. in the book: Modelling of Transport Phenomena in Crystal Growth, p.19-59, WIT Press, Southampton–Boston), 2000, eds. J. Szmyd & K. Suzuki.

[22] T. Umeda, T. Okane, W. Kurz, Phase selection during solidification of peritectic alloys, Acta Materialia **44**, 4209-4216 (1996).

[23] J. Schramm, Über eine neue phase in system eisen – zink, Zeitschrift für Metallkunde **29**, 222-225 (1937) (in German).

[24] W. Wołczyński, T. Okane, C. Senderowski, B. Kania, D. Zasada, J. Janczak-Rusch, Meta-stable conditions for diffusion brazing, Archives of Metallurgy and Materials **56**, 311-323 (2011).

[25] W. Wołczyński, Z. Pogoda, G. Garzeł, B. Kucharska, A. Sypień, T. Okane, Part I. Thermodynamic and Kinetic Aspects of the Hot Dip (Zn) – Coating Formation, Archives of Metallurgy and Materials **59**, 1223-1233 (2014).

[26] W. Wołczyński, Z. Pogoda, G. Garzeł, B. Kucharska, A. Sypień, T. Okane, Part II. Model for the Protective Coating Formation during Hot Dip Galvanizing, Archives of Metallurgy and Materials **59**, 1393-1404 (2014).

Received: 20 March 2014.